Deep-Sea Research I 57 (2010) 1206–1221

Contents lists available at ScienceDirect

Deep-Sea Research I

journal homepage: www.elsevier.com/locate/dsri

Numerical investigation on propulsion of the counter-wind current in the northern South China Sea in winter

Dongxiao Wang [a,*,1], Bo Hong [a,1], Jianping Gan [b], Hongzhou Xu [a]

[a] Key Laboratory of Tropical Marine Environmental Dynamics, South China Sea Institute of Oceanology, Chinese Academy of Sciences, Guangzhou 510301, China
[b] Department of Mathematics and Atmospheric, Marine and Coastal Environment Program, Hong Kong University of Science and Technology, Kowloon, Hong Kong, China

ARTICLE INFO

Article history:
Received 28 November 2009
Received in revised form
2 June 2010
Accepted 7 June 2010
Available online 23 June 2010

Keywords:
Northern South China Sea
Continental shelf/slope
Counter-wind current
Diagnostic analysis

ABSTRACT

The propulsion of the winter counter-wind current in the northern South China Sea (SCS) is investigated with a regional, three-dimensional, primitive equation model. This current is usually called the SCS Warm Current (SCSWC). Model results well reproduced the banded structure of the Guangdong coastal current, the SCSWC and the slope current from the coast to the slope in the northern SCS in the climatological data. The across-shelf flow is active in the shelf break area. Both onshore and offshore flows exist; the net across-shelf transport is shoreward throughout the year, and is larger in winter than in other seasons. The joint effect of baroclinicity and relief (JEBAR) is the dominant forcing of the across-shelf transport in the shelf break area. The major mass source of the SCSWC is the onshore-veered slope current. It is the JEBAR effect that supplies the necessary negative vorticity to maintain the slope current flowing across the isobaths and veering to the right hand to feed the SCSWC. Analyses of the momentum fields indicate that the onshore pressure gradient in the outer shelf balances the Coriolis force induced by the northeastward SCSWC in the frame of geostrophy. In winter, such an onshore pressure gradient is mainly provided by the strong density contrast between waters of the shelf and of the upper slope, which results from the Kuroshio intrusion via the Luzon Strait. The notable intrusion of the Kuroshio in winter is crucial for maintaining the density structure in the shelf break area and facilitates the set-up of the onshore pressure gradient over the outer shelf.

1. Introduction

The South China Sea (SCS) is a semi-enclosed marginal sea in the western Pacific Ocean (Fig. 1). The northern SCS is connected with the western Pacific Ocean and the East China Sea through the Luzon Strait and the Taiwan Strait, respectively. The Kuroshio flows along the east coast of Luzon and continues northward east of Taiwan after making a slight excursion into the northern SCS via the Luzon Strait. The continental shelf in the northern SCS is ENE–WSW oriented and 150–250 km wide, with the Dongsha Island located about 200 km offshore on a plateau over the upper continental slope. The strong northeast (winter) monsoon prevails in the SCS from October to March (Fig. 1). The winter counter-wind current in the northern SCS is a current that flows northeastward during the prevailing northeasterly wind in winter; it originates from the offshore area east of the Hainan Island, flows over the shelf/slope region, passes through the Taiwan Strait and finally enters the East China Sea according to Guan (1986) (dashed arrow line in Fig. 1). This current is also named the SCS Warm Current (SCSWC) for its temperature is generally higher than the surrounding waters in winter (Guan and Chen, 1964).

The SCSWC has drawn attention for decades because of its counter-wind feature in winter. The geostrophic flows at across-shelf transects reveal that there are three adjacent band-structured currents with reversed directions in the northern SCS from the coast to the slope in winter, namely the down-wind Guangdong coastal current, the SCSWC, and the southwestward slope current (Guo et al., 1985). In winter, the SCSWC can be as wide as 160–300 km; its velocity is lower in the west ($\sim$20 cm/s) and higher in the east ($\sim$50 cm/s), with much weaker flow in between ($\leq$10 cm/s) (Guan, 1986). In terms of hydrographic features, the isotherms over the outer continental shelf show an up-sloping inclination, and the stream axis of the SCSWC corresponds to a positive onshore gradient zone of density in January (Guan and Fang, 2006). When the southwest monsoon prevails in summer, the coastal current merges with the SCSWC to flow down-wind.

In winter there is a basin-wide cyclonic gyre in the SCS; in summer a cyclonic gyre remains north of about 12°N and an anticyclonic gyre prevails to the south (Wang et al., 2006). These basin-wide gyres are typically formed by the slope current along the northern and western continental margins in the SCS, i.e., the

* Corresponding author. Tel.: +86 20 8902 3204; fax: +86 20 8902 3205.
E-mail address: dxwang@scsio.ac.cn (D. Wang).
[1] Equally contributed to this paper.

0967-0637/$ - see front matter © 2010 Elsevier Ltd. All rights reserved.
doi:10.1016/j.dsr.2010.06.007

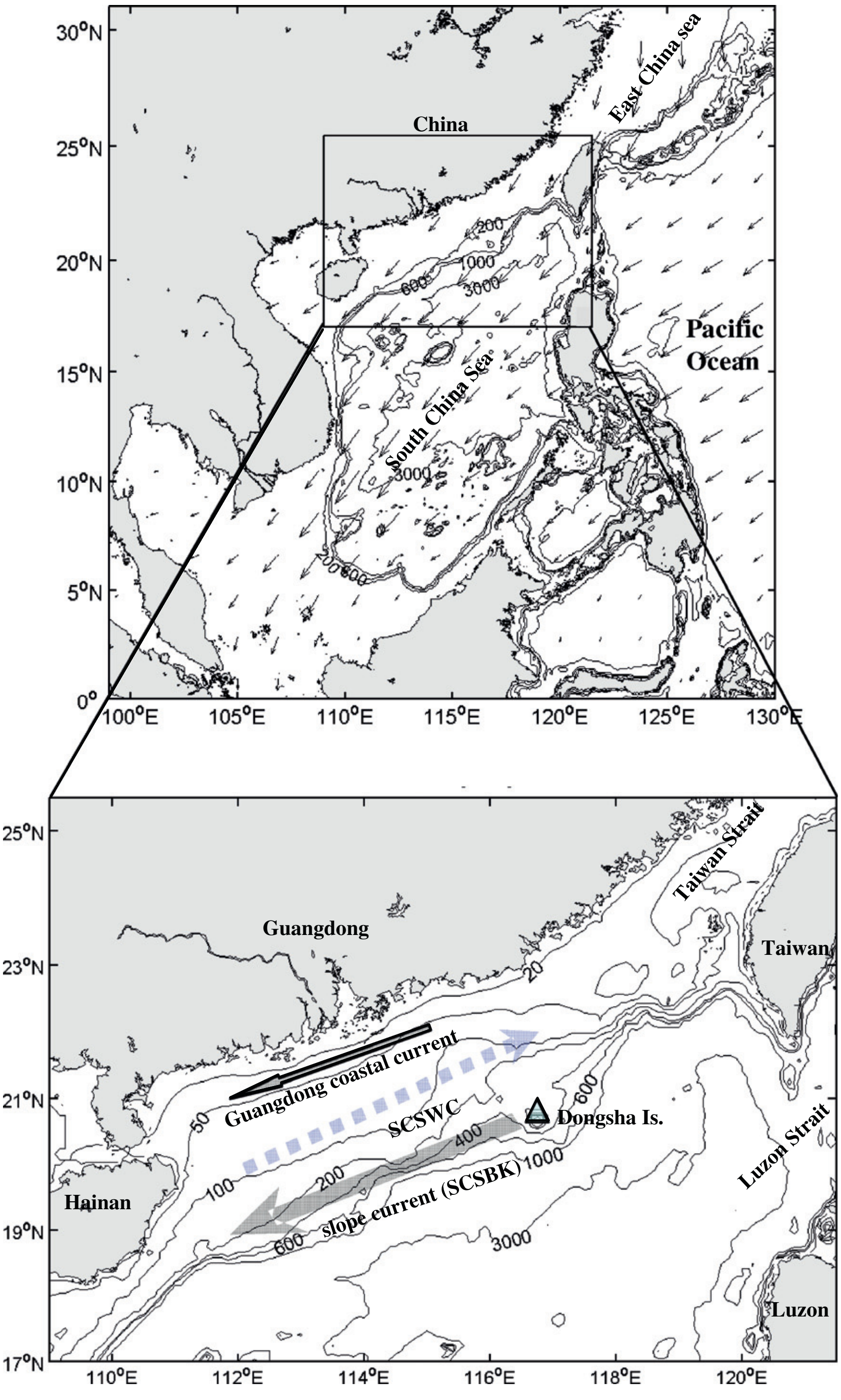

Fig. 1. Bathymetry of the South China Sea (SCS), with its northern part highlighted. The NCEP wind stress (Pa) climatology in January is superimposed. The circulation in the northern SCS continental shelf/slope in winter is denoted schematically: the down-wind Guangdong coastal current (thin arrow), the northeastward counter-wind current (also named the SCSWC; dashed arrow), the southwestward slope current (bold arrow). The triangle on the outer edge of the continental shelf represents the Dongsha Island.

SCS boundary current. In situ observations revealed that the southwestward slope current along the northern SCS continental margin exhibits obvious baroclinic structure and is much stronger than the SCSWC (Guo et al., 1985). Analyses of water mass distribution clarified that: when the northeast monsoon develops in late fall and winter, waters of the North Pacific origin flow into the interior SCS along the northern SCS continental slope and have a notable impact on the water characteristics of the entire northern SCS (Shaw, 1991; Qu, 2000). Recent moored current-meter and ship-board acoustic Doppler current profilers (ADCP) data confirmed that a branch of the Kuroshio intrudes into the Luzon Strait all year round (Liang et al., 2003). The intruded Kuroshio flow generally splits into two branches after its collision with the continental slope near the Dongsha Island. Since the southwestward branch flows along the edge of the shelf into the interior SCS (Qiu et al., 1984; Guan, 1985; Guo et al., 1985; Zhong, 1990), the southwestward slope current is often named as the SCS branch of the Kuroshio (SCSBK) in literature due to its obvious Kuroshio origin, and had been depicted in many numerical studies (e.g., Shaw and Chao, 1994; Li et al., 1996; Metzger and Hurlburt, 1996; Hsueh and Zhong, 2004; Xue et al., 2004). The northern branch turns clockwise toward the Kuroshio along the southern tip of Taiwan or flows into the Taiwan Strait through the Peng-Hu Channel (Liang et al., 2003).

The side-by-side presence of the SCSWC and the slope current draws much attention to oceanographers. By analyzing 10-year hydrographic data in the northern SCS, Zhong (1990) suggested that the SCSWC was a continuation of the SCSBK over the outer shelf, where the westward flowing SCSBK turned to the northeast in the region east of 114°E owing to the blocking effect of the bottom topography. They showed that unstable anticyclonic eddies could be discerned at the shelf break from the dynamic height fields. Fang and Zhao (1989) analyzed the long-term gauge data along the southeast coast of China and proposed that alongshore sea-surface elevation gradient was the main forcing for the SCSWC, since the contributions of wind stress, barometric pressure gradient and density gradient were all much smaller. However, their analyses could not explain the formation of the SCSWC that exists in the offshore area of Guangdong. Several other interpretations on the generation mechanism of the SCSWC have also been proposed. Guan and Chen (1964) also suggested that the SCSWC is guided by the bottom topography. The idealized numerical simulation of Ma (1987) suggested that the deflection of the slope current at the shelf break and the anticyclonic eddy in the northeastern SCS were the possible origination of the SCSWC. Periodical relaxation of the northeasterly wind associated with weather events would strengthen the SCSWC intermittently in winter (Chao et al., 1995). Hsueh and Zhong (2004) suggested that, in accordance with the arrested topographic wave theory, the pressure head (imposed by the incidence of the Kuroshio) along the continental shelf break generated a flow that resembled the SCSWC. Their results indicated that the SCSBK fed the SCSWC all along the shelf break through a weak onshore flow driven by the gradual drop in pressure in the SCSBK. Diagnostic analysis of Xue et al. (2004) revealed that upwelling over the northern SCS upper slope was important in maintaining the SCSWC. To what extent the SCSWC is steered by topography needs further investigation.

Year-round persistence and concentration over the outer edge of the continental shelf suggest that the SCSWC is insensitive to the local wind stress forcing. The adjacent hydrodynamic condition and bottom topography may be the main reasons that the SCSWC flows against the wind in winter. In the northern SCS, both convergence and divergence of the isobaths can be discerned (Fig. 1). From the view of potential vorticity conservation, bottom topographic variations may lead to vorticity generation when the flow cannot follow the isobaths. To the extent that the slope current runs onshore (offshore) across the isobaths, the corresponding squashing (stretching) of the water column must give rise to negative (positive) vorticity, i.e., right-hand (left-hand) tendency that leads an upslope (downslope) flow. These across-shelf transports are crucial for the mass maintenance of the SCSWC. Previous work already revealed that there is onshore flow in the northern SCS and the bottom topography (continental shelf break) has an important effect on this flow. However, how these across-isobath flows take place has not been answered. It requires thorough consideration of intrinsic vorticity budget and momentum balance in this area. In this paper, we use a three-dimensional, primitive equation model to reproduce the mean circulation in the northern SCS. We first validate the numerical simulations, and then focus on exploring the dynamical linkage between the SCSWC and its adjacent currents. The model and forcing fields are introduced in Section 2. Model results and in situ observations are compared in Section 3. After these model validations, the pattern of the SCSWC and its adjacent currents are shown in Section 4. Dynamic analyses are given in Section 5 to illustrate a possible forcing mechanism for the origination of the SCSWC. Conclusions are presented in Section 6.

2. Model and forcing functions

The numerical investigation is performed using the Princeton ocean model (POM), which is documented in detail by Blumberg and Mellor (1987). Briefly, POM is a hydrostatic, free-surface, sigma-coordinate, primitive equation model. With an embedded turbulence closure sub-model, it is well suited to study the nonlinear dynamics over a shallow, gently sloping continental shelf.

POM has been successfully used in numerical simulations of the SCS circulation (e.g., Chu et al., 1999; Yang et al., 2002; Xue et al., 2004; Gan et al., 2006). In order to avoid prescribing the Kuroshio intrusion through the Luzon Strait, the model domain is extended from the SCS to include part of the western Pacific Ocean and the southern East China Sea (Fig. 2). The ETOPO5 data set provided by the National Geophysical Data Center (NGDC) is used for prescribing the model bathymetry through bilinear interpolation. The horizontal orthogonal curvilinear coordinates are designed to be largely parallel and orthogonal to the along-shelf direction in the northern SCS, respectively. The model grids have spatial scales ranging from 13 km (in the northern SCS and the western boundary area of the Pacific Ocean) to 29 km (in the southern SCS) with an average of about 21 km. The vertical sigma-coordinate has 30 levels, which are logarithmically distributed with higher resolution near the surface and bottom to better resolve the surface and bottom Ekman layers. Horizontal diffusivities are parameterized using the Smagorinsky (1963) formulation with a scaling coefficient of 0.2. Bottom stress, τ_b, is calculated by a quadratic law with variable drag coefficient, which has a minimum value of 0.0025.

The diagnostic calculations are used to simulate the circulation in each month. The temperature and salinity are fixed to the initial fields during the simulation, and monthly surface and lateral kinematic forcing are applied. The model is integrated from a state of rest. This approach has been proven to be efficient for diagnostic studies (e.g., Mellor et al., 1982).

The model is initialized by the climatological hydrographic data provided by the World Ocean Atlas 2001 (WOA01) at 0.25° resolution (Boyer et al., 2005). WOA01 is one of the best available gridded data sets in this area; however, it has limitations due to the large-scale smoothing used on the historical observations. This may influence the accuracy of our diagnostic simulation results somewhat, it does not, however, alter the circulation pattern. Surface wind stresses are calculated from the monthly climatology of the Nation Centers for Environmental Prediction/National Center for Atmospheric Research (NCEP/NCAR) reanalysis fields (Kalnay et al., 1996). The lateral forcing of the model is provided by the simple ocean data assimilation (SODA) reanalysis products (Carton and Giese, 2008), using one-way radiative nesting scheme proposed by Flather (1976). The normal component of the external mode barotropic velocity is

$$\overline{u}_B = \overline{u}_n^{obc} - \sqrt{\frac{g}{H}}(\eta - \eta^{obc}) \qquad (1)$$

where $\overline{u}^{obc}$ and η^{obc} represent the external velocity and surface elevation data specified at the open boundary, respectively; g and H are the gravity acceleration and local water depth, respectively. It provides a good connection between the model circulation and its surrounding one. A sponge layer is used for absorbing any undesired boundary reflection, as suggested by Israeli and Orszag (1981). The internal velocities at each level are free to adjust geostrophically to the density field. In this way the Kuroshio is

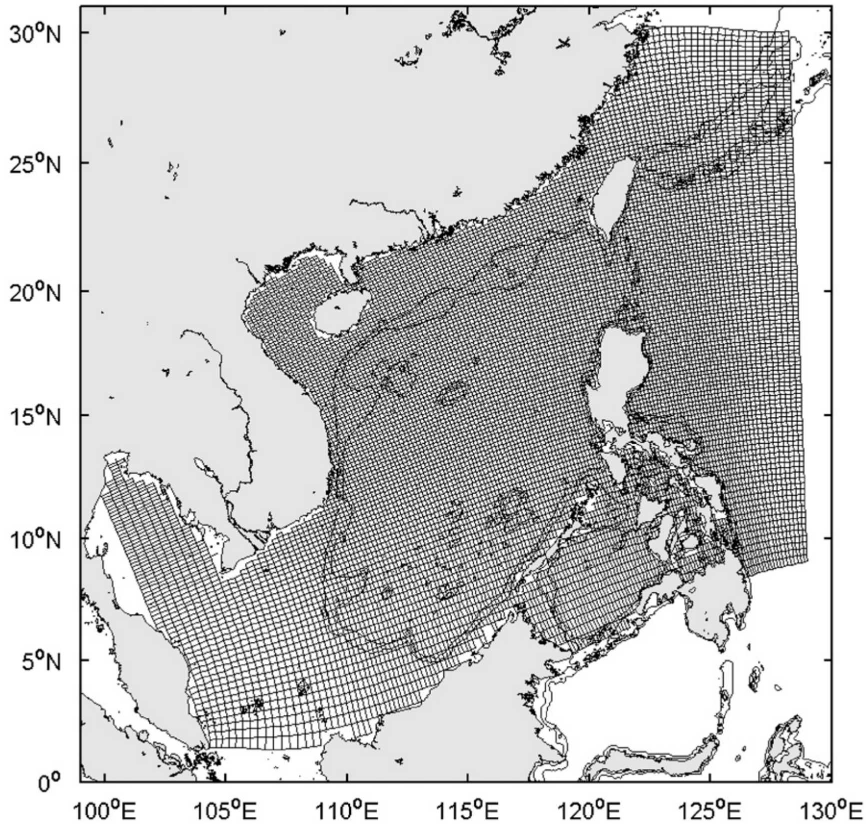

Fig. 2. Model domain and computational grids, superimposed with 200 and 1000 m isobaths.

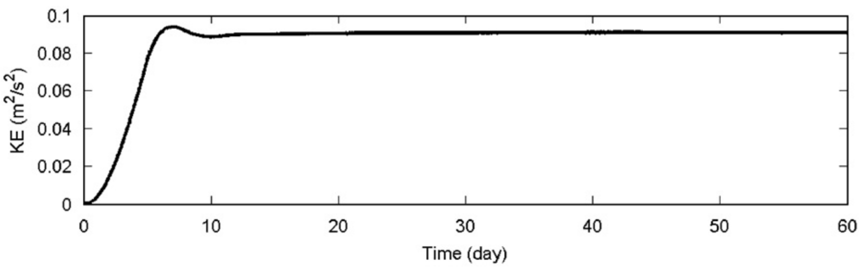

Fig. 3. Temporal evolution of the volume-averaged kinetic energy (KE) (m^2/s^2) in January.

generated properly in the inner domain of our model instead of being artificially prescribed near the Luzon Strait. The Kuroshio transport east of the Philippine Island had been validated by Hong and Wang (2008). Note that tidal forcing is not considered in this study.

Time series of volume-averaged kinetic energy (KE) is used to estimate the time scale for the model to reach its quasi-equilibrium state (Fig. 3). After the fast spin-up process, the model comes into a low frequency adjustment. The volume-averaged KE is almost constant after 40-day integration, which means a 60-day diagnostic run is long enough for the model to achieve a reasonable quasi-equilibrium state under the climatological external forcing. The fields presented in the following are the averages of the model results in the last 5 days, which are reasonably assumed to be non-transient. Winter, spring, summer and fall are defined as periods from December to February, March to May, June to August and September to November, respectively. The seasonal fields showed below are the averages over the corresponding months.

3. Validation of model results

Observational data for the velocity fields in the SCS is very limited. Guan (1986) summarized the observed current measurements at 10-m depth off the southeast China coast in winter, reproduced here in Fig. 4b. The data covered the coastal and shelf areas in the northern SCS and also the area around the Taiwan Island. The velocity data obtained during different cruises are indicated by different velocity vectors. In order to validate model results, the modeled velocity field at 10-m depth in winter is presented in Fig. 4a in a similar fashion as the observation in Fig. 4b. Comparison between Fig. 4a and b indicates that modeled current field is in similar pattern with that shown in the observed results. It can be readily seen that both the modeled and observed SCSWC originated from the offshore area east of the Hainan Island, and flew nearly consistently along the shelf towards the Taiwan Strait, against the winter monsoon. Since the scale of the current vector in Fig. 4b is not available, we cannot compare the current intensity between model results and

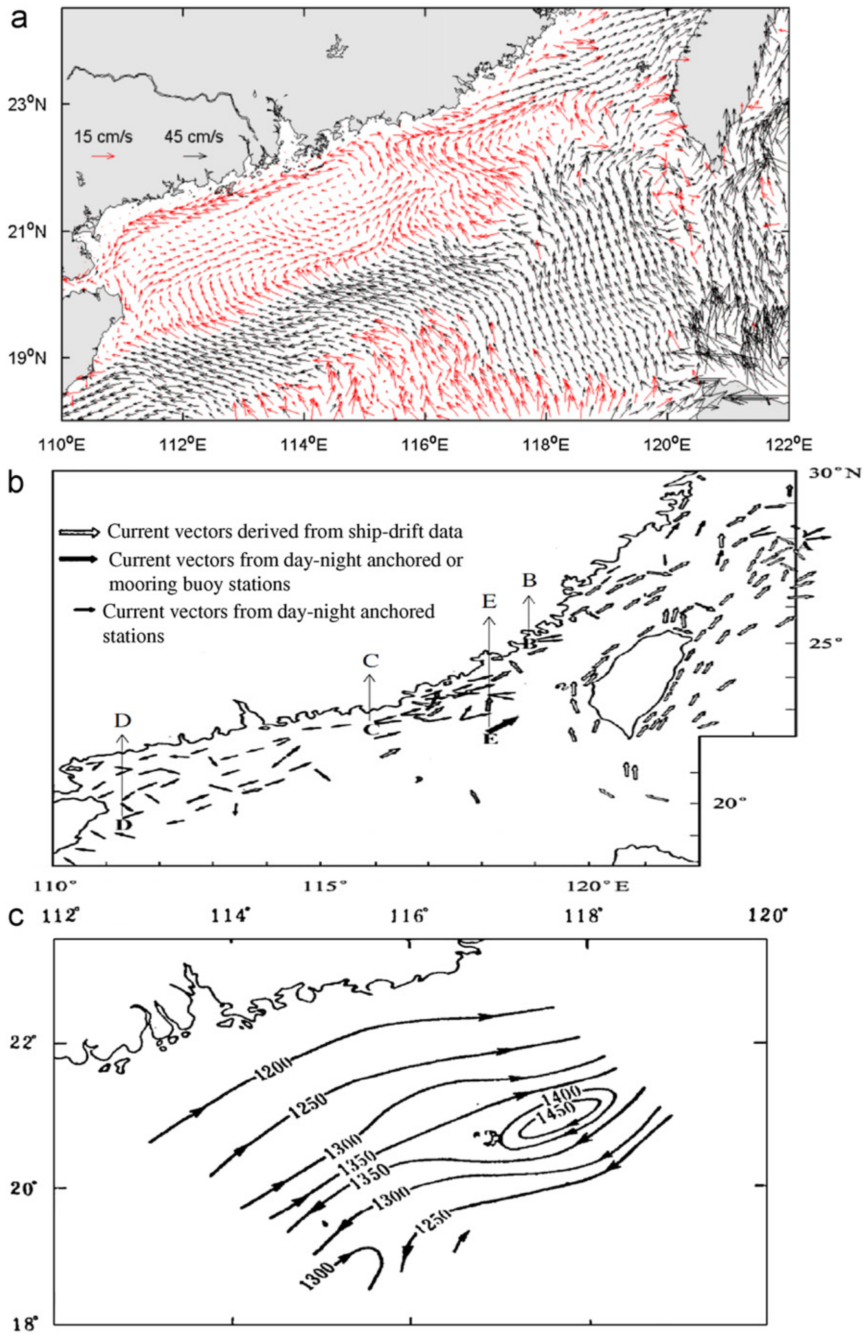

Fig. 4. Comparisons between model results and observations in winter: (a) modeled velocity at 10-m depth (note the magnitude difference of the red and black vectors for display purpose); (b) observed currents at 10-m depth (reproduced from Guan, 1986), with markers of D, C, E and B from the west to the east denoting the stations depicted in Fig. 5; (c) sea-surface dynamic topography (calculations based on the in situ hydrographic data) relative to 500 dB surface (dyn. mm; reproduced from Guo et al., 1985). (For interpretation of the references to color in this figure legend, the reader is referred to web version of this article.)

observations here. The modeled down-wind Guangdong coastal current can be seen clearly over the inner shelf, as in the observation. The modeled SCSWC flew side by side with the slope current in the opposite direction, which can be validated by the dynamic calculation of Guo et al. (1985) reproduced here in Fig. 4c. Based on the in situ hydrographic data in winter, Guo et al. (1985) calculated the sea-surface dynamic topography relative to 500 db surface (Fig. 4c). The SCSWC and slope current could be clearly identified from the sea-surface dynamic topography field. In winter, the upper-layer circulation in the northern SCS is cyclonic with intensified boundary current along the continental slope. Part of the intruded Kuroshio is entrained by the slope current flowing southwestward along the slope, which is in an agreement with the result of Qu et al. (2000). The remaining part of the intruded Kuroshio is veered northeastward after it reaches the continental slope near the Dongsha Island, and finally returns to the Pacific or goes into the Taiwan Strait (Fig. 4b). The modeled currents around Taiwan also show a pattern similar to the composite current map of Liang et al. (2003).

Comparisons are also made between the modeled and observed vertical structure of the residual currents in winter at mooring stations B, C, D and E (locations are marked in Fig. 4b) located offshore of the south China coast (Fig. 5). Fig. 5b is reproduced from Guan (1986). The corresponding water depths of

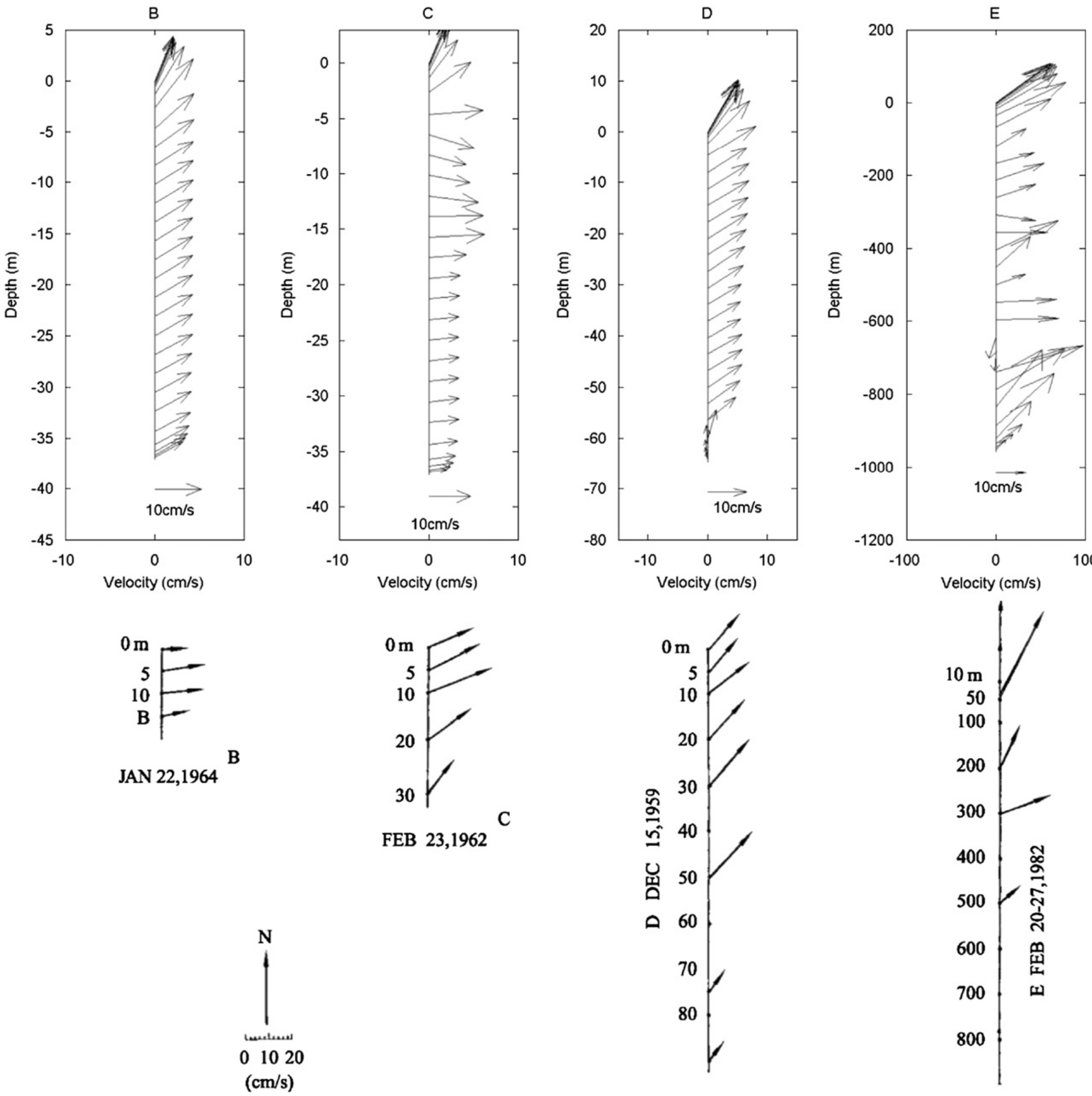

Fig. 5. Vertical structure of the currents at Stations B, C, D and E (locations are marked in Fig. 4b) off the South China coast. The corresponding water depths of these stations are 37, 37, 65 and 953 m, respectively. The upper (lower) panel is the modeled (observed) results. The observations (reproduced from Guan, 1986) were obtained through day–night anchored and mooring station measurements in winter. The dates of each observation are also shown in the lower panel.

these stations are 37, 37, 65 and 953 m, respectively. Except for the surface currents at individual stations where the Ekman drift induced by the northeasterly wind may prevail, both the modeled and the observed current directions in the whole water column at these four stations are basically toward the northeast. These indicate the currents shown in Fig. 4b are representative for the current conditions not only at 10-m depth but also below this depth in these areas. A deficiency of the modeled currents lies in the amplitude. The model underestimates the velocity by about 50% at Stations B, C and D. The systematic underestimate of the SCSWC may be the result of the disparity of initial density fields (due to large-scale smoothing of the WOA01 climatological data) and different forcing (climatological forcing is used in this study, while observations were taken as snapshots), among other things.

Our model-data comparisons are relatively qualitative owing to the limitation of available observations. Despite the discrepancies shown in Figs. 4 and 5, it does not detract from the fact that our model is able to capture the features of these currents in the northern SCS, and the results are suitable for diagnostic studies. Next, the model results are used to investigate the circulation in the northern SCS and to explore possible mechanisms for the formation of the SCSWC. For clarity, we only show the fields in the domain covering the northern SCS continental shelf/slope.

4. Pattern of SCSWC and its adjacent currents

The seasonal-mean velocity fields depth-integrated in the upper 1000 m are shown in Fig. 6, superimposed on the corresponding sea-surface elevation fields. Also included in the figure are vectors of the NCEP climatological wind stress in order to show the pattern of the monsoon forcing in each season. The most prominent feature on the continental shelf is the

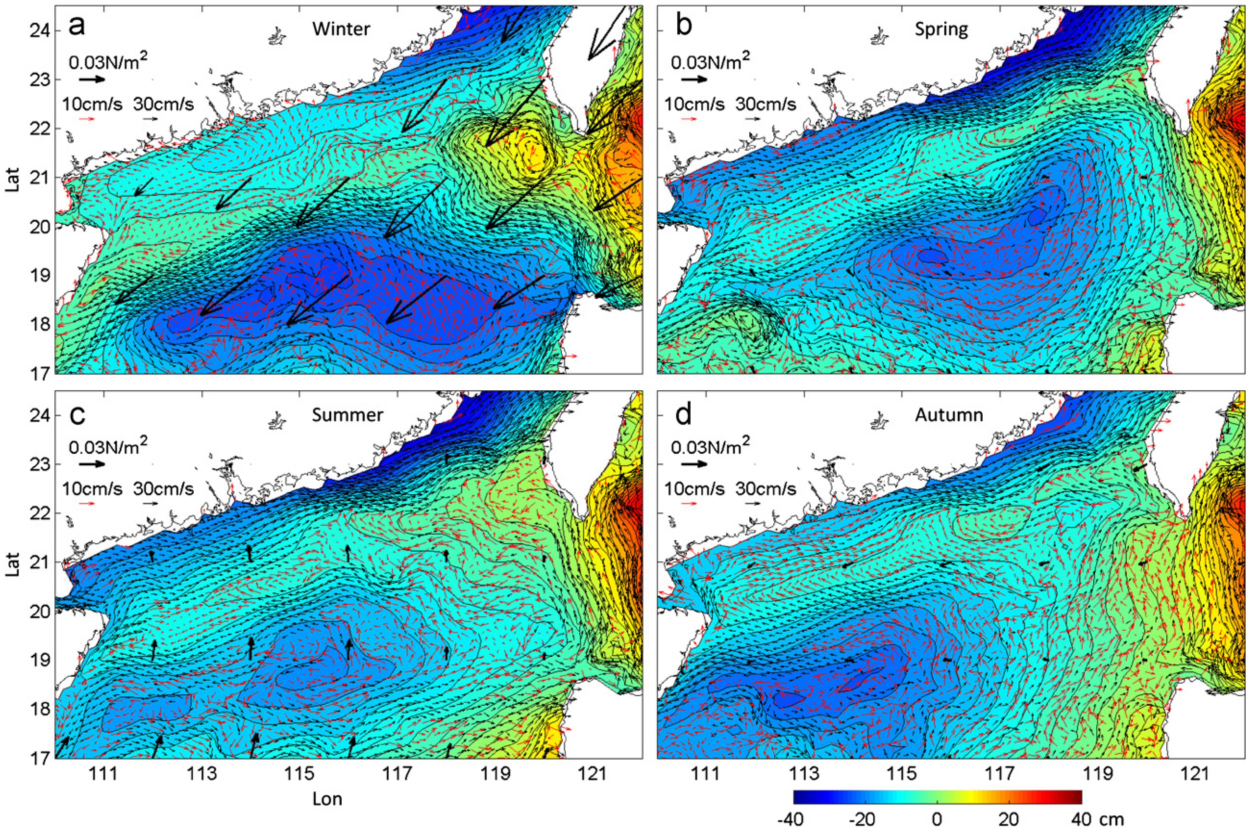

Fig. 6. Annual cycle: the sea-surface elevation field (cm; contour interval being 2 cm); modeled velocity integrated in the upper 1000 m (cm/s; thin vectors; note the magnitude difference of the red and black vectors for display purpose); and NCEP wind stress (N/m^2; heavy vectors plotted every 2°): (a) winter; (b) spring; (c) summer and (d) autumn. The color bar represents the scale of sea-surface elevation in cm (for interpretation of the references to color in this figure legend, the reader is referred to the web version of this article).

year-round high sea-surface elevation belt along the outer edge of the continental shelf. Along the flank of this belt, the slope current and the SCSWC flow in opposite directions. Across-shelf flow, which is weaker than the alongshore flow, can be discerned across the high sea-surface elevation belt. The SCSWC is the weakest in winter when the winter monsoon prevails. It is strengthened in summer when the coastal current merges into it under the forcing of summer monsoon. The most notable intrusion of Kuroshio occurred in winter, which is consistent with previous studies of Shaw (1991) and Qu et al. (2000). The northern edge of the basin-wide cyclonic gyre is confined by the continental shelf and forms relatively strong southwestward slope current. The strongest (weakest) slope current exists in winter (summer) when the cyclonic gyre is the strongest (weakest).

These across-shelf movements are very important for exploring the mass source of the SCSWC. The question is what forces the flow crossing the isobaths. The forcing should be set up in such a way that it provides the necessary negative (positive) relative vorticity that forces water to flow onshore (offshore). The possible mechanism will be addressed next.

5. Dynamical analyses

The ocean current is expected to flow, at the first-order approximation, along the f/H contours (where f is Coriolis parameter, and H is water depth) when the relative vorticity is much smaller than the planetary vorticity. However, we notice that the slope current in the northern SCS does not exactly follow the f/H contours; instead, it intersects with these contours at the outer edge of the continental shelf. The interaction between bottom slope and density field arises when the baroclinic transport has a component along the depth gradient. Previous studies suggested that, in the real ocean, the transport across the f/H contours of the continental slope was highly related with the joint effect of baroclinicity and relief (JEBAR; Sarkisyan and Ivanov, 1971). Sakamoto and Yamagata (1996) first explicitly applied the dynamic (i.e., time-dependent) aspects of JEBAR to study seasonal variation of the wind-driven gyre. Generally, JEBAR represents the torque exerted on the fluid column by the joint action of density and topographic gradients to deviate it from following the f/H contours (e.g., Holland, 1973; Mellor et al., 1982; Huthnance, 1984; Myers et al., 1996; Isobe, 2000; Guo et al., 2003). To clarify this, we investigate the correlation between the transport across the f/H contours and JEBAR effect in the northern SCS in the frame of vorticity balance equation.

5.1. JEBAR effect on across-shelf transport

We start from analyzing the voriticity balance equation, in which the contribution of sea-surface elevation to the water column depth is included. Cross-differentiate the vertically integrated momentum equation will result in a vertically integrated vorticity balance equation

$$\overbrace{\frac{\partial}{\partial t}\left[\frac{\partial}{\partial x}\left(\frac{\overline{v}}{D}\right)-\frac{\partial}{\partial y}\left(\frac{\overline{u}}{D}\right)\right]}^{a}+\overbrace{u\frac{\partial}{\partial x}\left(\frac{f}{D}\right)+v\frac{\partial}{\partial y}\left(\frac{f}{D}\right)}^{b}$$

$$=\underbrace{J\left(\Phi,\frac{1}{D}\right)}_{c}+\underbrace{curl\left(\frac{F}{D}\right)}_{d}\underbrace{-curl\left(\frac{A}{D}\right)}_{e}+\underbrace{curl\left(\frac{\tau_a}{\rho_0 D}\right)}_{f}\underbrace{-curl\left(\frac{\tau_b}{\rho_0 D}\right)}_{g} \quad (2)$$

where $(\overline{u},\overline{v})$ represents the vertically integrated velocity, $J(\Phi,\frac{1}{D})$is the JEBAR term,$\Phi=\int_{-H}^{\eta} zg\rho/\rho_0 dz$ is the potential energy, ρ is the density,η is the surface elevation, $D=H+\eta$ is water column depth;$(\tau_x,\tau_y)_0$ and $(\tau_x,\tau_y)_b$ are the surface and bottom stresses, respectively;$F=F_x i+F_y j$ and $A=A_x i+A_y j$ are the vertically integrated horizontal diffusion term and the nonlinear advection term, respectively. The left-hand side of Eq. (2) includes (a) the tendency term and (b) advection of the geostrophic potential vorticity (APV) term. The right-hand side of Eq. (2) includes (c) the JEBAR term, (d) diffusion term (DIF), (e) advection term (ADV), (f) surface-stress torque and (g) bottom-stress torque. Using the model results we can calculate each term in Eq. (2). In the quasi-steady state, the APV term should be balanced by the sum of those terms on the right-hand side of Eq. (2) because the tendency term should approximately be zero in the quasi-steady state.

Since the change in topography overwhelms the change in planetary vorticity, the transport across the f/D contours (APV term) is nearly identical to the cross-isobath transport. In the continental shelf/slope area, if the APV term equals to zero, the transport is exactly along the isobaths. If the APV term is positive, the transport is in the onshore direction and the slope current tends to intersect the isobaths and to climb up the continental slope (e.g., Isobe, 1999). If the APV term is negative, the transport is in the offshore direction and the slope current tends to veer toward the deep ocean (e.g., Sakamoto and Yamagata, 1996; Guo et al., 2003).

Fig. 7 displays the spatial distribution of each term in Eq. (2). The APV term is much larger at the edge of the shelf than in other areas, which means the across-shelf transport (APV $\neq 0$) is fairly active in the whole northern SCS shelf break area. The across-shelf transport also exists in the inner shelf, though much weaker. Both the APV term and the JEBAR term are dominant and show similar fractal-like spatial structure along the shelf break. In the shelf break area, the typical magnitude of the APV term is about $2\times10^{-9}\,s^{-2}$ ($1\times10^{-9}\,s^{-2}$) in winter (summer), which is very close to that of the JEBAR term. The APV term can be mainly balanced by the JEBAR term in most of the area. Among the remaining terms, the contribution of advection term is secondary along the shelf break. The bottom-stress torque and surface-stress torque become dominant only in the shallower area.

5.1.1. Basic forcing of across-shelf transport

Because the across-shelf transport is fairly active in the shelf break area, the region bounded by 200 and 600-m isobaths is first selected for further analyses. The vertical profile of the across-shelf flow together with the vorticity terms are shown in Fig. 8 (only the results west of 117°E are shown for clarity). The velocity profile and the vorticity terms are all averaged in the across-shelf direction between 200- and 600-m isobaths. Water in this bounded region can be regarded as the upstream origin of the onshore (offshore) right-hand (left-hand) veered flow at the shelf break. The results indicate both the onshore and offshore flows alternatively exist in the shelf break area. It is easy to find that each onshore (offshore) flow corresponds to the positive (negative) APV term, which is consistent with previous theoretical analyses. The term-by-term analyses suggest the most dominant contribution comes from the JEBAR term, which balances the APV term. Although there are seasonal variations in the magnitude of these terms, their spatial patterns are relatively stable. It can be confirmed from these analyses that the JEBAR effect is the dominant forcing of the across-shelf transport in the shelf break area. Such profiles of across-shelf flow and vorticity terms are also sampled in the shallower area. The directions of the resulting across-shelf flow also show variability, but the JEBAR effect is no longer the most dominant force of the across-shelf transport. The contributions of

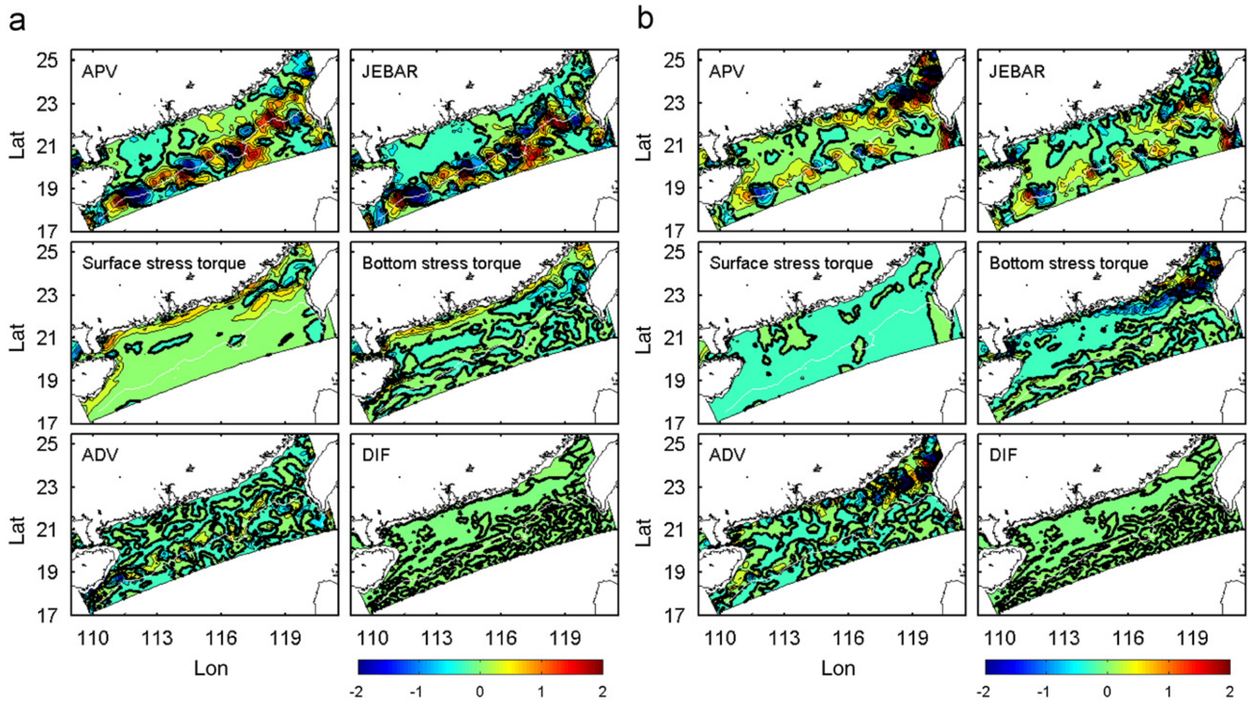

Fig. 7. Spatial distribution of the vorticity terms in winter (a) and summer (b). The bold black lines represent zero contours. The contour interval is $0.3\times10^{-9}\,s^{-2}$. The 400-m isobath (white line) is superimposed on each panel.

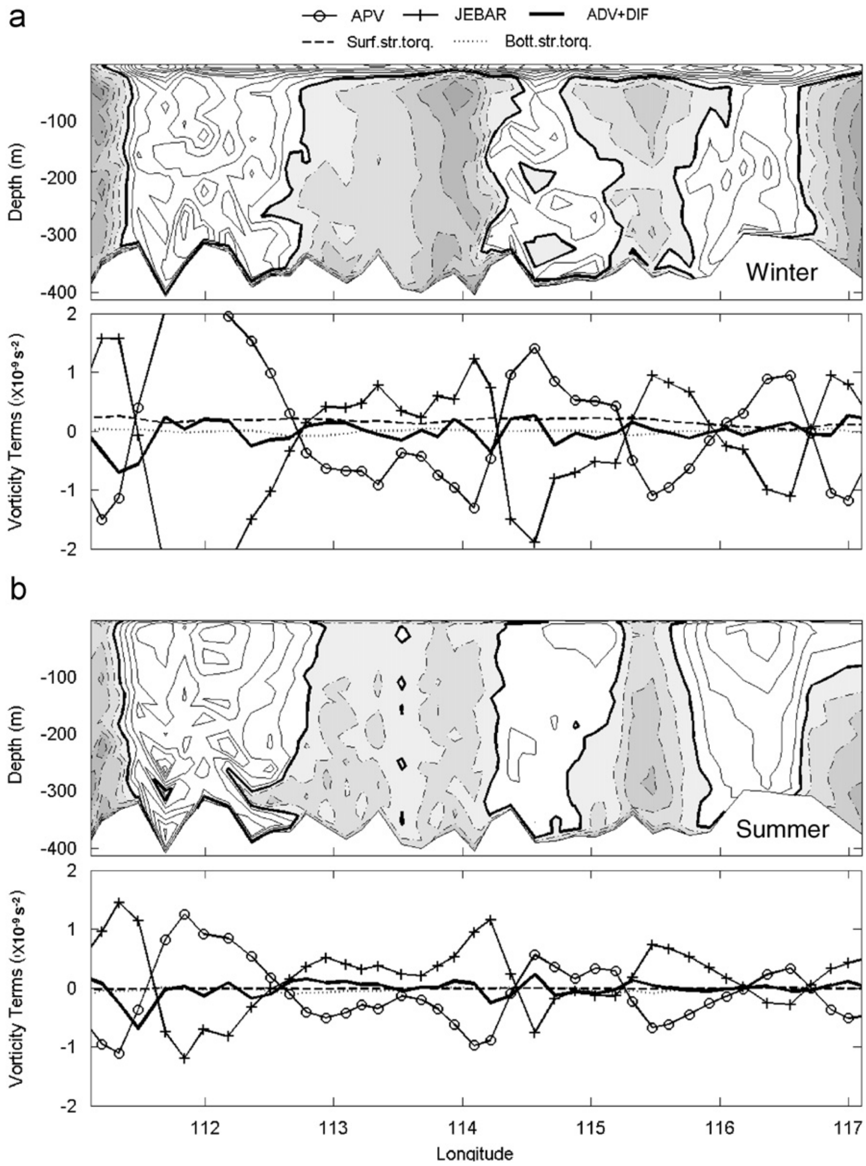

Fig. 8. Vertical profile for the across-shelf velocity (upper; cm/s) and vorticity ($\times 10^{-9}\,s^{-2}$; lower) terms balance along the continental slope in the northern SCS in winter (two upper panels) and summer (two lower panels). The velocity and the vorticity terms are the results averaged in the across-shelf direction between the 200- and 600-m isobaths. The shaded area in the velocity profile denotes offshore flow. The contour interval is 2 cm/s. The terms on the right-hand side of Eq. (2) are rearranged to the left-hand side of the equation for display purpose.

advection, surface-stress torque (in winter) and bottom-stress torque are all considerable in the shallower area.

Since both the onshore and offshore flows exist along the shelf, it is necessary to evaluate the net across-shelf transport to see if there is such an onshore (offshore) transport from the deep sea (inner shelf) that could provide the required mass to feed a current like the SCSWC flowing out of the SCS through the Taiwan Strait all year round. For this purpose, we integrate the across-shelf volume transport along the 200-m isobath in the northern SCS. The results indicate the net across-shelf volume transport is shoreward (>0) all year round and becomes stronger in winter (Fig. 9a). Again, we integrate the vorticity terms in the same way and show the results in Fig. 9b and c. The integrated APV term (>0) shows the same trend of variation as the net across-shelf transport, which also becomes larger in winter. When the largest magnitude of the integrated APV term ($3\times10^{-9}\,s^{-2}$) appears in December, the net onshore transport can reach its maximum value of 1.28 Sv. When the integrated APV term has its smallest value in March, the net onshore transport also reaches its minimum value of 0.67 Sv. The variations of the remaining terms in Eq. (2) clearly indicate that the major balance is still between the APV term and the JEBAR term. Therefore, the net onshore transport is mainly forced by the JEBAR effect, which is stronger in winter; in another word, it is the JEBAR effect that mainly supplies the necessary negative vorticity to maintain the slope current flowing across the isobaths and veering to the right hand to feed the SCSWC. Net across-shelf transport is also estimated in the shallower area. The results (figure not shown) indicate that the direction of the across-shelf transport changes with time (dominated by wind forcing) and the transport is much lower than that of the SCSWC. Such unstable and relatively weak across-shelf flow in the shallower area is not sufficient to provide the necessary mass source to maintain a current like the SCSWC.

5.1.2. *Factors influencing JEBAR effect*

From the mathematical expression of the JEBAR term $\left(J(\Phi,\frac{1}{D})=\frac{-1}{D^2}\left(\frac{\partial\Phi}{\partial x}\frac{\partial D}{\partial y}-\frac{\partial\Phi}{\partial y}\frac{\partial D}{\partial x}\right)\right)$, we know that the magnitude and

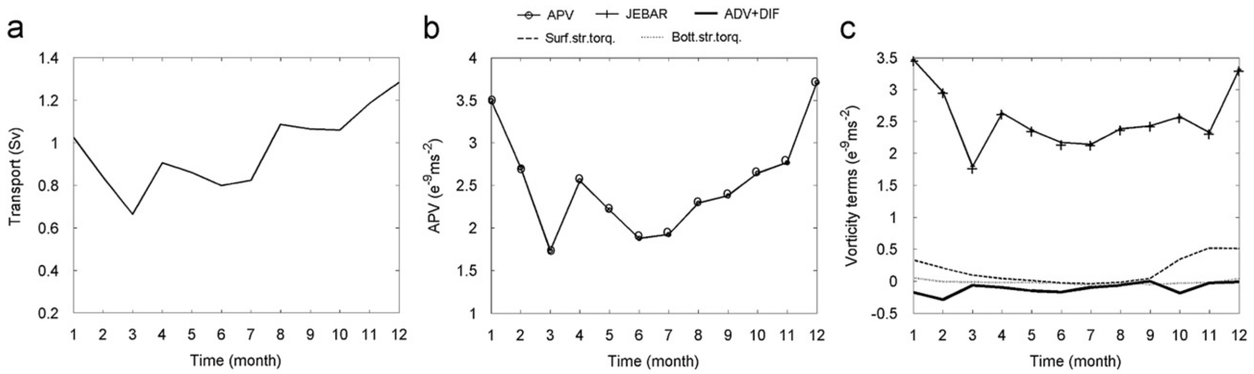

Fig. 9. Monthly across-shelf volume transport (Sv; 1 Sv $=10^6$ m^3 s^{-1}) (a), the APV term ($\times 10^{-9}$ s^{-2}) (b), and the remaining terms ($\times 10^{-9}$ s^{-2}) on the right-hand side of Eq. (3) (c) integrated along the 200-m isobath in the northern SCS between 111.1°E and 117.2°E. The positive values in (a) indicate northward volume transport.

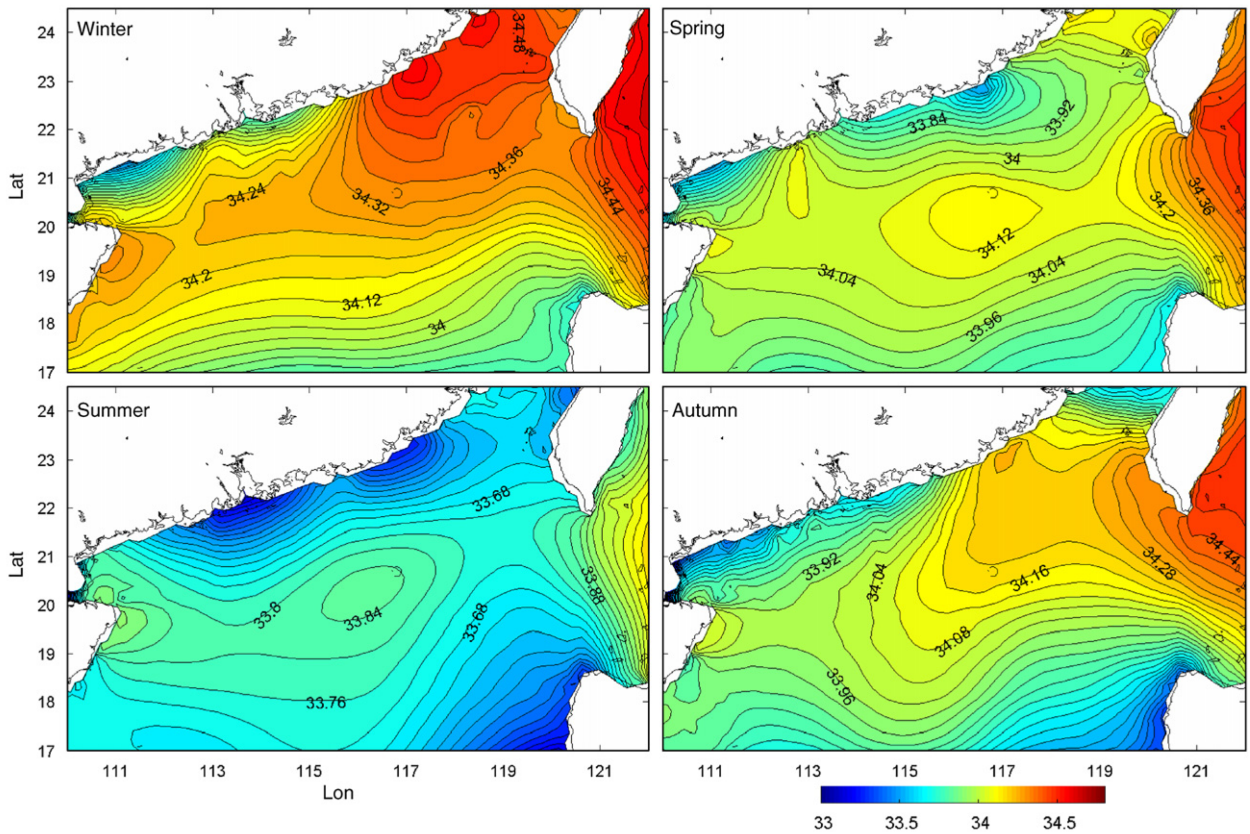

Fig. 10. Seasonal-mean salinity distribution at 10-m depth. The contour interval is 0.04.

sign of the JEBAR effect (consequently, the across-shelf transport) are determined by both the topographic gradient and the horizontal density gradient. This is the reason why the horizontal density gradient cannot alter the total transport in the water column in a flat-bottom ocean model. It is easy to understand that the changes of the JEBAR term in different seasons (e.g., Figs. 8 and 9) result from the changes in horizontal density gradients in the northern SCS. Fig. 10 presents modeled salinity fields (same as the model's initial field since it is unchanged in the diagnostic calculation). The typical seasonal variation of density field in the shelf break area can be reflected: the water is more saline in winter than in other seasons. Since the most notable intrusion of the Kuroshio occurs in winter, the resulted along-slope density gradient in the northern SCS shelf break area is stronger in winter than in other seasons. Therefore, the JEBAR term is relatively larger in winter than in other seasons.

5.2. *Effect of lateral forcing*

The density contrast between waters of the shelf and of the upper slope is particularly strong in the northern SCS owing to the Kuroshio intrusion through the Luzon Strait. Previous studies revealed that the circulation in the northern SCS is largely governed by the Kuroshio intrusion dynamics (e.g., Xu et al., 1982; Metzger and Hurlburt, 1996; Qu et al., 2000). The effect of lateral forcing can be evaluated by a sensitivity run that is only forced by the lateral forcing. The annual-mean fields of the model results shown in Section 4 (produced by the diagnostic calculation) are used to initialize the sensitivity run. The surface wind forcing is turned off. The climatological annual-mean SODA data are used to provide the lateral forcing for the sensitivity run. Upstream scheme is adopted for the open boundary conditions of temperature and salinity, in which the prescribed climatological annual-mean values at the boundaries are advected into the model domain for the inflow condition. The momentum open boundary condition is the same as the control run described in Section 2. With the annual-mean lateral forcing only, the model is run prognostically (temperature and salinity fields adjust at the same time with the momentum field) for 330 days. The results averaged in the last 5 days are used for the analyses shown next.

Fig. 11a presents the velocity fields depth-averaged in the upper 400 m. When the local wind effect is absent, the basin-wide cyclonic gyre disappears and the dynamics dominated by the Kuroshio intrusion stand out. The intruded Kuroshio splits into two branches after it impinges onto the continental shelf near the Dongsha Island, consistent with previous observations (e.g., Zhong, 1990). The northeastward branch returns to the Pacific along the southern tip of the Taiwan Island. The southwestward branch (i.e., the SCSBK) flows along the continental slope into the interior SCS, forming a slope current that appears to be more divergent than that in the control run. The onshore flow can be clearly discerned at the shelf break. A northeastward current that resembles the SCSWC flows along the outer shelf. In the inner shelf, the current tends to veer offshore as the inner shelf widens, especially east of 115°E, as addressed by Gan et al. (2009). The corresponding salinity fields sampled at 10 and 50-m depths are shown in Fig. 11b and c. There is a high salinity belt extending

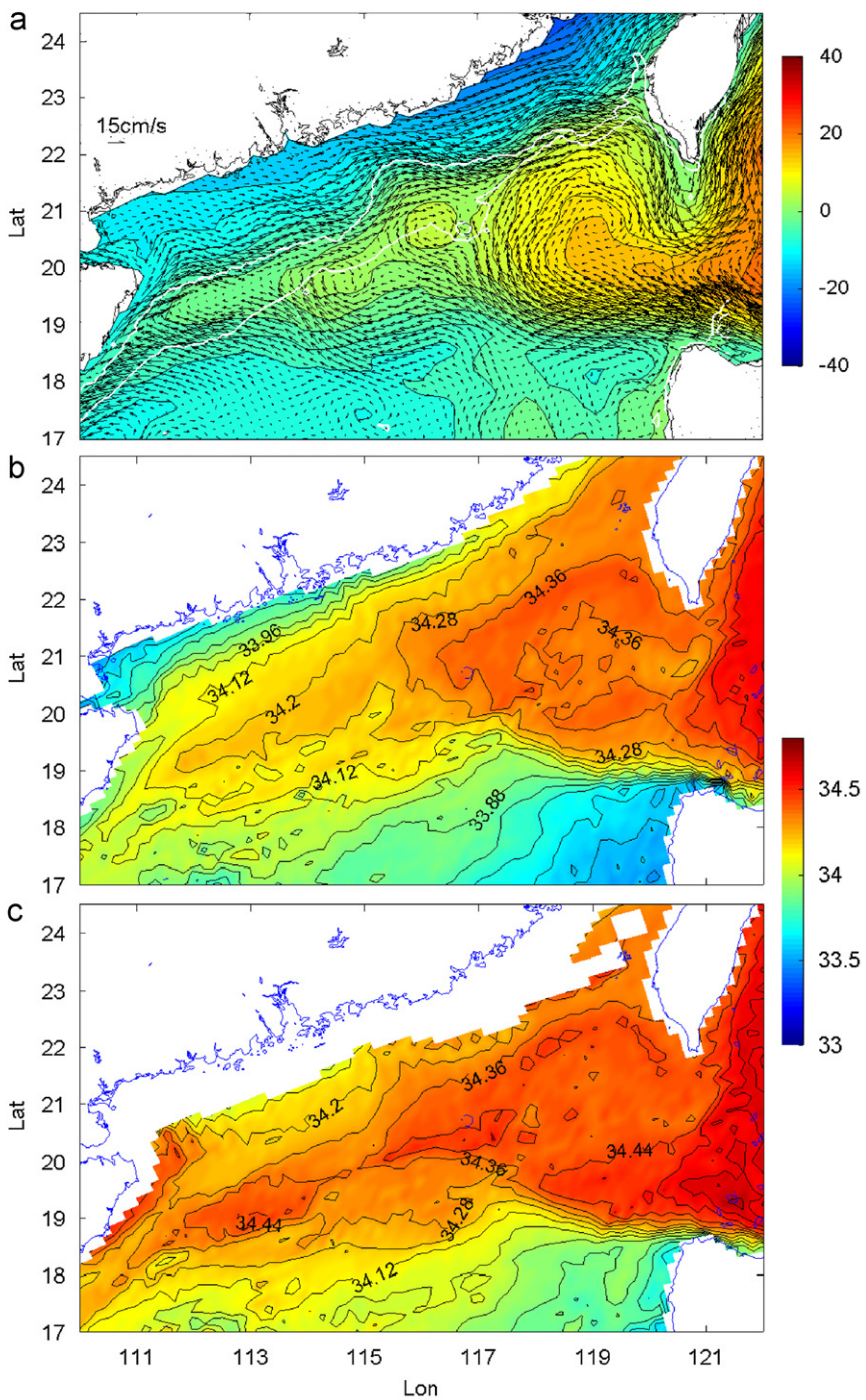

Fig. 11. Results for the sensitivity run: (a) velocity field depth-integrated in the upper 400 m, superimposed on the sea-surface elevation field; (b) salinity field at 10-m depth and (c) salinity field at 50-m depth. The contour interval for the sea-surface elevation and salinity field is 2 cm and 0.08, respectively.

from east to west along the shelf break. The pattern of the high salinity belt is similar to the high sea-surface elevation belt shown in Fig. 11a.

Comparing the results of the sensitivity run with the annual mean fields (figure not show) generated from the control run outputs (i.e., Fig. 10), the water is more saline in the sensitivity run (Fig. 11b and c) than in the control run. The Kuroshio intrusion (indicated by high-salinity water mass) in the sensitivity run is stronger than in the control run, in terms of annual mean. Since the western Pacific Ocean is the only source of high salinity water to the northern SCS, it is clear that the Kuroshio intrusion through the Luzon Strait facilitates the set-up of the high-salinity belt (consequently the across-shelf density gradient) along the outer shelf. The local wind effect generates the basin-wide cyclonic gyre in the northern SCS, which is bounded by the continental shelf and forms the slope current. The slope current and SCSBK actually merge together in the control run.

The spatial distribution of the vorticity terms in the sensitivity run is shown in Fig. 12. The patterns of these terms are similar with those in Fig. 7; the intensity and dominant area of the APV term and JEBAR term, however, show some variations. The tendency term (not shown) approximates to zero everywhere, which indicates the sensitivity run has reached a quasi-steady state. The magnitude of the APV term is still larger at the shelf break (which indicates the across-shelf transport is more active) than in other areas. Examination on the across-shelf transport in the shelf break area (sampled between 200- and 600-m isobaths) is shown in Fig. 13a. The onshore flow occupies most part of the area. Since it has been shown in the previous section that the across-shelf transport is mainly forced by the JEBAR effect at the shelf break area, it is clear that the density field maintained by the Kuroshio intrusion is capable of facilitating the net onshore transport through the JEBAR effect to feed the SCSWC flowing out of the SCS. Since there is clearly an offshore flow in the shallower area, we also sample the across-shelf velocity field and vorticity terms between 50- and 100-m isobaths (Fig. 13b). When the offshore (onshore) flow appears, the APV term is largely negative (positive), which is consistent with the theoretical analyses. However, the across-shelf flow in the shallower area is forced by the combined effect of JEBAR, ADV and bottom-stress torque. The

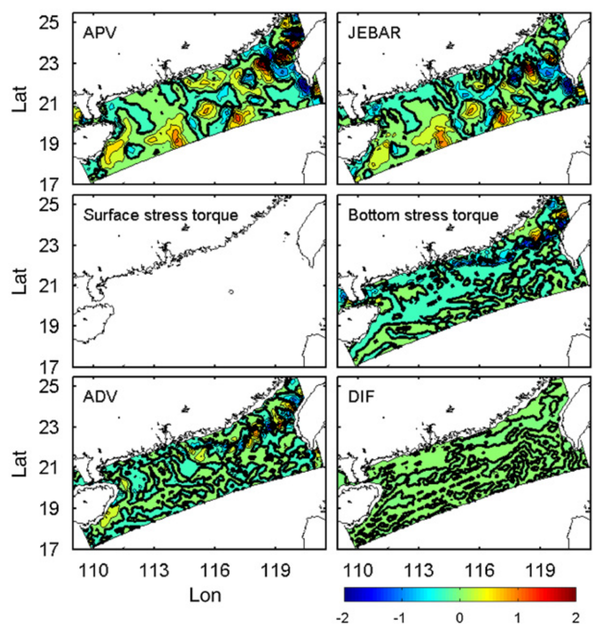

Fig. 12. Spatial distribution of the vorticity terms for the sensitivity run. The bold black lines represent the zero contours. The contour interval is $0.3\times10^{-9}\,\mathrm{s}^{-2}$.

net transport in this area is offshore; its total transport is, however, much lower than that of the SCSWC and is not sufficient for feeding the SCSWC. Therefore, the mass source of the SCSWC mainly comes from the onshore-veered slope current. The contribution of across-shelf flow in the inner shelf is secondary.

5.3. Momentum constraint for northeastward SCSWC

Although it has been revealed that the JEBAR effect plays an important role in forcing the slope current across the isobaths to feed the SCSWC, it is still not sufficient to answer the question what forces the SCSWC to flow against the wind in winter. Analyses of the momentum budget are presented in this section in order to identify the dynamic regime in the shelf/slope area. The depth-integrated along-shelf (u-component; positive value directed northeastward) and across-shelf (v-component; positive value directed onshore) momentum equation can be represented by

$$\overbrace{u_t}^{a}+\overbrace{V\cdot\nabla u}^{b}\overbrace{-F_x}^{c}\overbrace{-fv}^{d}+\overbrace{P_x}^{e}\overbrace{-(K_m u_\sigma)_\sigma}^{f}=0 \tag{3a}$$

$$\overbrace{v_t}^{a}+\overbrace{V\cdot\nabla v}^{b}\overbrace{-F_y}^{c}\overbrace{+fu}^{d}+\overbrace{P_y}^{e}\overbrace{-(K_m v_\sigma)_\sigma}^{f}=0 \tag{3b}$$

where V is the velocity vector with components (u,v,w), P is pressure, K_m is vertical viscosity coefficient, F_x and F_y represent the horizontal diffusion terms in along-shelf and across-shelf directions, respectively (see detailed definition in Blumberg and Mellor, 1987), and $\sigma=(z-\eta)/H$is the vertical σ-coordinate. The terms in the momentum equations include (a) tendency, (b) advection term (ADV), (c) horizontal diffusion term (DIF), (d) Coriolis term (COR), (e) pressure gradient (PRE), (f) surface stress (SUF) and (g) bottom stress (BOT). For simplicity, the terms in Eqs. (3a) and (3b) are not intended to represent the strict mathematical expression of the momentum equations. All the terms are evaluated in a local curvilinear coordinate, and the results in the quasi-steady state are examined next.

Fig. 14 displays the spatial distribution of depth-integrated momentum terms (for the control run) in the across-shelf direction. The pressure gradient is onshore in the continental shelf area, whereas it is offshore on the upper continental slope. Comparing the patterns of the SCSWC and its adjacent currents, it can be found that the northeastward SCSWC appears where the pressure gradients are onshore. In the shelf break area, the dominant momentum balance is between pressure gradient and Coriolis force. The surface and bottom stresses play an important role only in the inner shelf area. From the view point of kinematics, the onshore pressure gradient is balanced by the Coriolis force induced by the SCSWC in the frame of geostrophy. The onshore pressure gradient is very important for providing the momentum constraint for the SCSWC flowing against the wind in winter.

In order to explore the dominant cause of the onshore pressure gradient at the outer shelf, we calculate the across-shelf density gradient in winter (Fig. 15). The density gradient is onshore (offshore) in the area where the SCSWC (the slope current) occupies. The in situ hydrographic observations show precisely such density configuration in winter (e.g., Guan, 1978; Guo et al., 1985; Zhong, 1990). Since $\frac{\partial p}{\partial x_i}=\frac{\partial}{\partial x_i}\int_z^\eta \rho g\,dz'=\rho(\eta)g\frac{\partial\eta}{\partial x_i}+\int_z^\eta g\frac{\partial\rho'}{\partial x_i}dz'$, the across-shelf pressure gradient is caused by both the sea-surface slope and the density gradient in the across-shelf direction. In the control run, the onshore sea-surface slope is steeper in summer than in winter owing to the Ekman drifting (Fig. 6). Although the onshore sea-surface slope is weakened when the winter monsoon prevails (the piling up of coastal water forced by the wind tends to set up the offshore sea-surface slope),

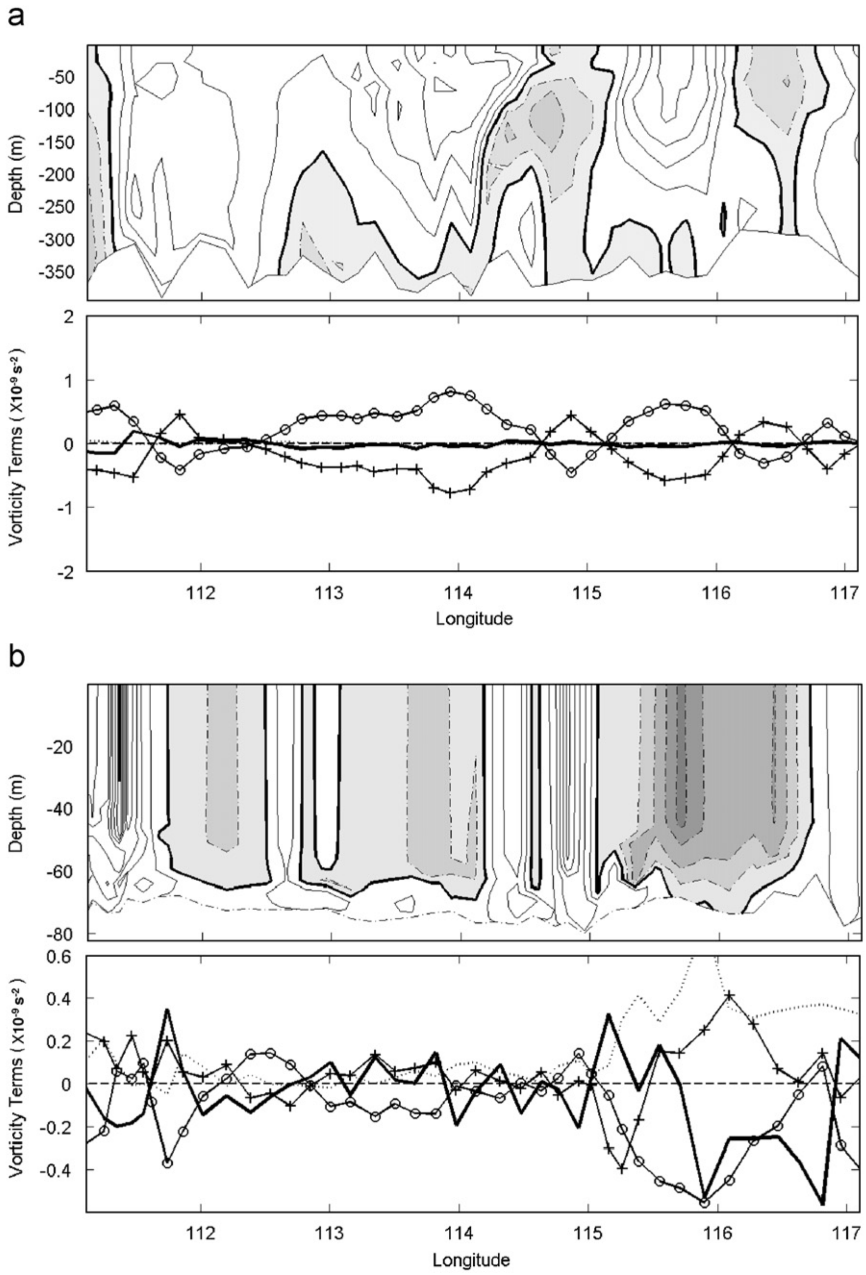

Fig. 13. Same as Fig. 8 except for the sensitivity run: (upper panels) averaged in the across-shelf direction between the 200- and 600-m isobaths; (lower panels) averaged in the across-shelf direction between the 50 and 100 m isobaths.

the Kuroshio intrusion is relatively stronger in winter than in other seasons (Shaw, 1991; Qu et al., 2000). Thus the across-shelf density gradient is crucial in winter for setting up the required onshore pressure gradient to induce the SCSWC flowing against the wind.

6. Discussion and conclusions

The purpose of this paper is to provide a dynamical interpretation for the propulsion of the winter counter-wind current in the northern SCS, the SCSWC. Using one-way nested scheme, a regional high-resolution general circulation model is adopted to reproduce the circulation in the SCS together with the western boundary current of North Pacific Ocean. With the climatological lateral and surface forcing, the model is run diagnostically to derive the circulation in each month from the climatological hydrographic data. The results have a good representation of the circulation in the northern SCS, in particular the side-by-side presence of the SCSWC and the slope current, the vertical structure of the SCSWC, and the Kuroshio intrusion. The slope current is the northern boundary of the basin-wide cyclonic gyre, which exists in the northern SCS all year round. During the notable intrusion of the Kuroshio in winter, the slope current is the combination of the cyclonic gyre boundary current and the SCSBK.

The across-shelf flow is fairly active in the whole northern SCS shelf break area, which is very important to the across-shelf exchange in the northern SCS. Analyses on the profiles of across-shelf velocity and vorticity balance equations reveal that each onshore (offshore) flow corresponds to a positive (negative) APV term. The JEBAR effect is the dominant forcing of such across-shelf transport. Although both the onshore and offshore flows can be discerned at the shelf break, the net across-shelf transport integrated along the 200-m isobath in the northern SCS (111.1–117.2°E) is shoreward all year round and stronger in winter. It is the JEBAR effect that mainly supplies the necessary negative vorticity to maintain the slope current flowing across the isobaths and veering to the right hand to feed the SCSWC. The seasonal variations of JEBAR result from the changes of horizontal density gradient. The water around the shelf break is much saline in winter than in other seasons. A sensitivity run without wind forcing reveals that the Kuroshio intrusion through the Luzon Strait facilitates the set-up of the onshore density gradient. The density field maintained by the Kuroshio intrusion is capable of generating the net onshore transport through the JEBAR effect. Examinations of the inner shelf indicate that the across-shelf transport is forced by the combined effect of JEBAR, ADV and bottom-stress torque. The net across-shelf transport in the shallower area is much lower than that of the SCSWC and changes its direction with time. Such unstable and relatively weak flow is not sufficient to feed a current like SCSWC. Thus the dominant mass source of the SCSWC is the onshore-veered slope current, which is mainly forced by the JEBAR effect. The contribution of water in the inner shelf is secondary.

Analyses on the momentum field indicate there is a high pressure belt along the shelf break of the northern SCS throughout the year. The resulting pressure gradient is onshore in the continental shelf area. Momentum term balances reveal that the onshore pressure gradient is balanced by the Coriolis force induced by the SCSWC in the frame of geostrophy. The across-shelf pressure gradient is caused by both sea-surface slope and the density gradient in the across-shelf direction. The spatial distribution of the across-shelf density gradient suggests there is an onshore density gradient in the area occupied by the SCSWC. In winter, the onshore sea-surface slope is greatly weakened when

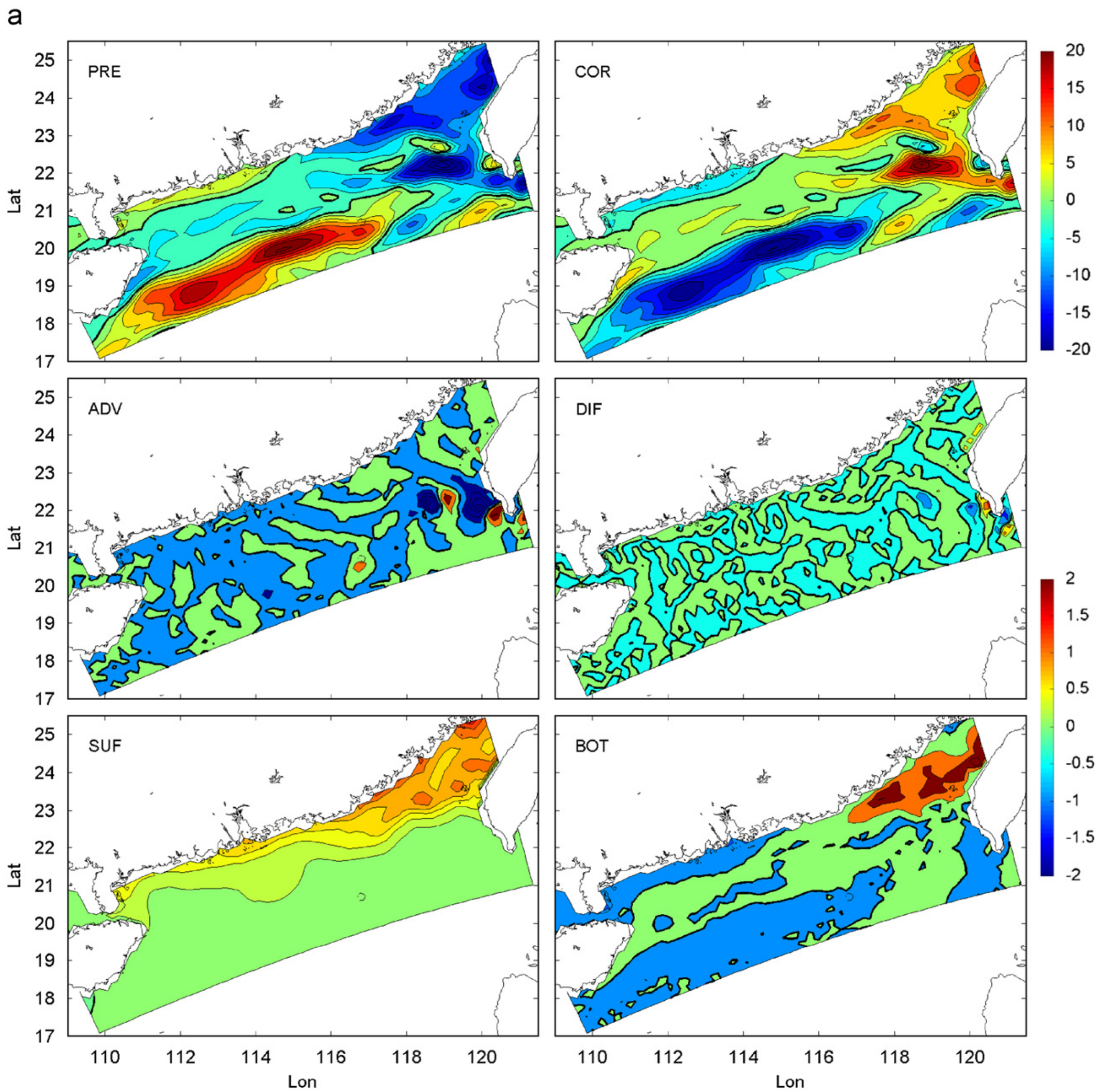

Fig. 14. Across-shelf momentum term balance in winter (a) and summer (b). The bold black lines represent the zero contours. The counter interval is 3×10^{-6} m s^{-2}.

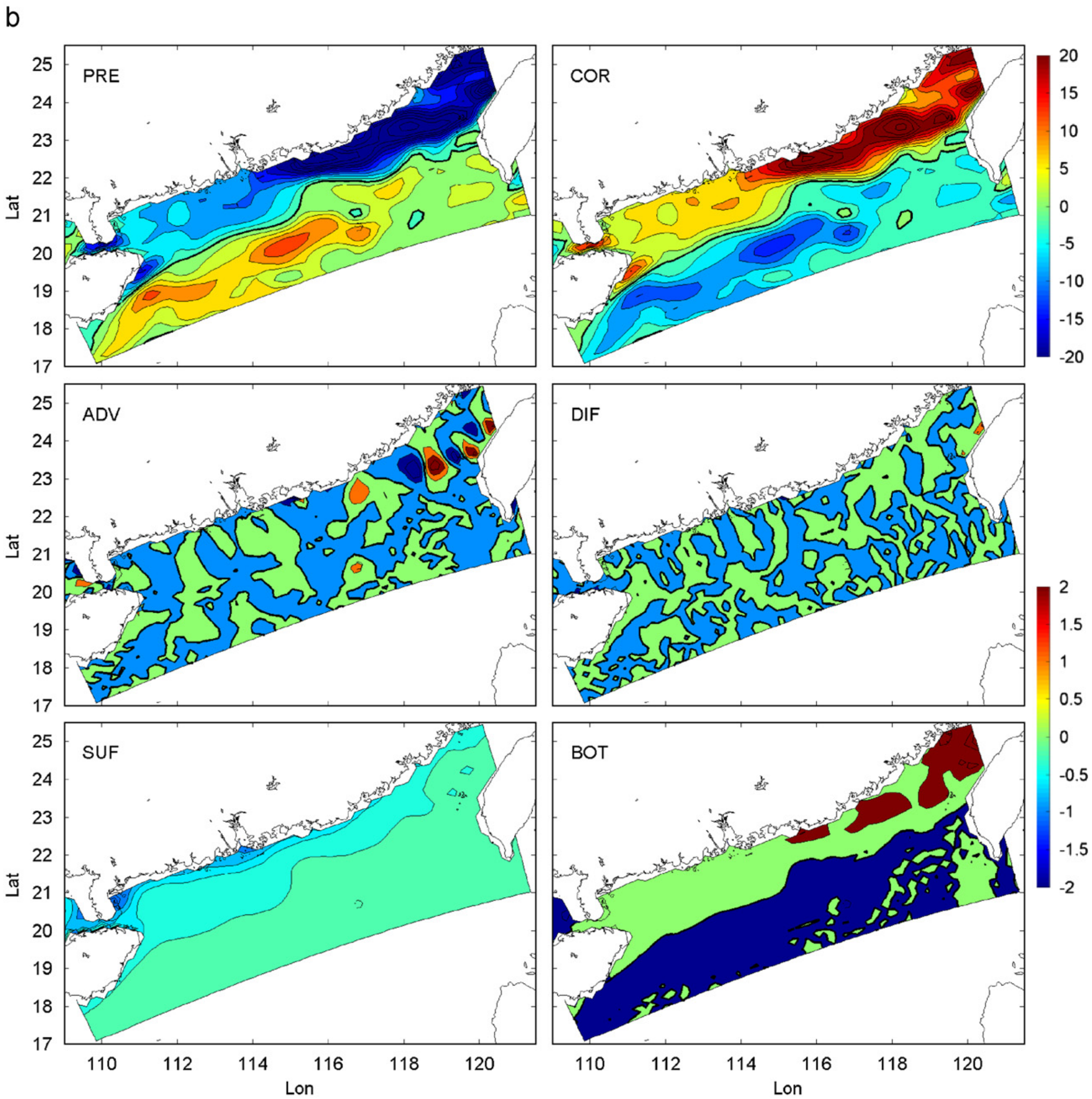

Fig. 14. (*Continued*)

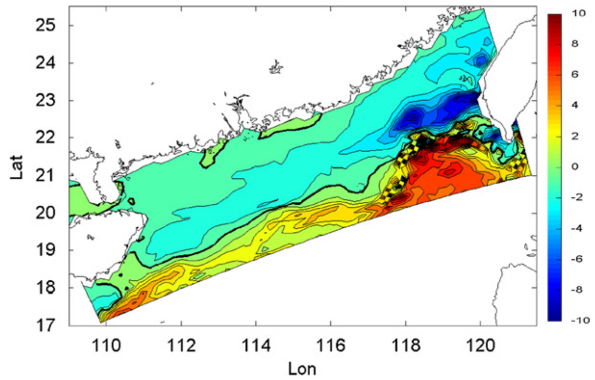

Fig. 15. Across-shelf density gradient in winter. The bold black lines represent the zero contours. The counter interval is 1×10^{-6} m s^{-2}.

the northeast monsoon prevails, whereas the Kuroshio intrusion is relatively stronger at that time. The onshore density gradient maintained by the intruded Kuroshio water is crucial for setting up the required onshore pressure gradient to induce the SCSWC flowing against the wind in winter.

Finally, the important role played by the JEBAR effect indicates it is necessary to maintain the density structure over the northern SCS continental shelf in order to achieve a realistically modeled across-shelf transport. The results of the sensitivity run suggest the intruded Kuroshio water (usually indicated by high-salinity water mass) is crucial for facilitating such density configuration (especially for setting up the onshore density gradient in winter). In addition, good representation of the continental slope bathymetry is also important for the model to reproduce the SCSWC. The information on the depth-dependent distribution of the potential vorticity is required for further understanding the baroclinic-bathymetric interaction in the northern SCS continental slope, for which robust observational hydrographic data is needed. The method used in this paper could be applied in other shelf break areas to study the across-shelf transport process. The counter-wind flow could occur in other shelf areas when the JEBAR effect plays a key role in the shelf break area to force the across-shelf transport and the density field is suitably maintained to set up the required onshore pressure gradient to induce the current flowing against the wind.

Acknowledgements

This study was supported by the Chinese Academy of Sciences (KZCX1-YW-12-01 and KZSW2-YW-214) and the National Natural Science Foundation (40625017, U0733002 and 40830851). We would like to thank the editor and two anonymous reviewers for comments that helped to improve the manuscript. We also want to thank Dr. Zuojun Yu for helping to improve the writing of the manuscript.

References

Boyer, T., Levitus, S., Garcia, H., Locarnini, R., Stephens, C., Antonov, J., 2005. Objective analyses of annual, seasonal, and monthly temperature and salinity for the World Ocean on a 1/4° grid. International Journal of Climatology 25, 931–945.

Blumberg, A.F., Mellor, G.L., 1987. A description of a three-dimensional coastal ocean circulation model. Three-Dimensional Coastal Ocean Models. Coastal and estuarine sciences. In: Heaps, N. (Ed.), American Geophysical Union, Washington, D.C. 4, 1–16.

Carton, J.A., Giese, B.S., 2008. A reanalysis of ocean climate using simple ocean data assimilation (SODA). Monthly Weather Review 36, 2999–3017.

Chao, S.Y., Shaw, P.T., Wang, J., 1995. Wind relaxation as a possible cause of the South China Sea Warm Current. Journal of Oceanography 51 (1), 111–132.

Chu, P.C., Edmons, N.L., Fan, C.W., 1999. Dynamical mechanisms for the South China Sea seasonal circulation and thermohaline variabilities. Journal of Physical Oceanography 29, 2971–2989.

Fang, G., Zhao, B., 1989. A note on the main forcing of the northeastward flowing current off the southeast China coast. Progress in Oceanography 21, 363–372.

Flather, R.A., 1976. A tidal model of the northwest European continental shelf. Memoires Societe Royale des Sciences de Liege 6 (10), 141–164.

Gan, J., Li, H., Curchitser, E.N., Haidvogel, D.B., 2006. Modeling South China Sea circulation: response to seasonal forcing regimes. Journal of Geophysical Research 111, C06034. doi:10.1029/2005JC003298.

Gan, J., Li, L, Wang, D., Guo, X., 2009. Interaction of a river plume with coastal upwelling in the northeastern South China Sea. Continental Shelf Research 29, 728–740.

Guan, B.X., 1985. Some temporal and spatial distribution features of the wintertime counter-wind current in the northern South China Sea. Oceanologia et Limnologia Sinica 16 (6), 429–437 (in Chinese with English abstract).

Guan, B.X., 1978. The warm current in the South China Sea—a current flowing against the wind in winter in the open sea off Guangdong Province. Oceanologia et Limnologia Sinica 9 (2), 117–127 (in Chinese with English abstract).

Guan, B.X., Fang, G., 2006. Winter counter-wind currents off the southeastern China coast: a review. Journal of Oceanography 62, 1–24.

Guan, B.X., 1986. Evidence for a counter-wind current in winter off the southeast coast of China. Chinese Journal of Oceanology and Limnology 4 (4), 319–332.

Guan, B.X., Chen, S., 1964. The current systems in the near-sea area of China Seas. Initial Report 5, 1–85 (in Chinese).

Guo, X., Hukuda, H., Miyazawa, Y., Yamagata, T., 2003. A triply nested ocean model for simulating the Kuroshio—roles of horizontal resolution on JEBAR. Journal of Physical Oceanography 33, 146–169.

Guo, Z., Yang, T., Qiu, D., 1985. The South China Sea Warm Current and the SW-ward current on its right side in winter. Tropical Oceanology 4 (1), 1–9 (in Chinese).

Holland, W.R., 1973. Baroclinic and topographic influences on the transport in western boundary currents. Geophysical Fluid Dynamics 4, 187–210.

Hong, B., Wang, D., 2008. Sensitivity study of the seasonal mean circulation in the northern South China Sea. Advances in Atmospheric Sciences 25, 824–840.

Hsueh, Y., Zhong, L., 2004. A pressure-driven South China Sea Warm Current. Journal of Geophysical Research 109, C09014. doi:10.1029/2004JC002374.

Huthnance, J.M., 1984. Slope currents and "JEBAR". Journal of Physical Oceanography 14, 795–810.

Isobe, A., 1999. On the origin of the Tsushima Warm Current and its seasonality. Continental Shelf Research 19, 117–133.

Isobe, A., 2000. Two-layer model on the branching of the Kuroshio Southwest of Kyushu, Japan. Journal of Physical Oceanography 30, 2461–2476.

Israeli, M., Orszag, S.A., 1981. Approximation of radiation boundary conditions. Journal of Computational Physics 41, 115–135.

Kalnay, E., Kanamitsu, M., et al., 1996. The NCEP/NCAR 40-year reanalysis project. Bulletin of the American Meteorological Society 77, 437–471.

Li, R.F., Guo, D., Zeng, Q., 1996. Numerical simulation of interrelation between the Kuroshio and the current of the northern South China Sea. Progress in Natural Science 6, 325–332.

Liang, W.D., Tang, T., Yang, Y., Ko, M., Chuang, W., 2003. Upper-ocean currents around Taiwan. Deep-Sea Research II 50, 1085–1105.

Ma, H., 1987. On the winter circulation of the northern South China Sea and its relation to large oceanic current. Chinese Journal of Oceanology and Limnology 5 (1), 9–21.

Mellor, G.L., Mechoso, C., Keto, E., 1982. A diagnostic calculation of the general circulation of the Atlantic Ocean. Deep-Sea Research 29, 1171–1192.

Metzger, E.J., Hurlburt, H.E., 1996. Coupled dynamics of the South China Sea, the Sulu Sea, and the Pacific Ocean. Journal of Geophysical Research 101, 12331–12352.

Myers, P.G., Fanning, A.F., Weaver, A.J., 1996. JEBAR, bottom pressure torque, and Gulf stream separation. Journal of Physical Oceanography 26, 671–683.

Qiu, D., Yang, T., Guo, Z., 1984. A westward current in the northern South China Sea in summer. Tropical Oceanology 3, 65–73 (in Chinese).

Qu, T., 2000. Upper-layer circulation in the South China Sea. Journal of Physical Oceanography 30, 1450–1460.

Qu, T., Missudera, H., Yamagata, T., 2000. Intrusion of the North Pacific waters into the South China Sea. Journal of Geophysical Research 105, 6415–6424.

Sakamoto, T., Yamagata, T., 1996. Seasonal transport variations of the wind-driven ocean circulation in a two-layer planetary geostrophic model with a continental slope. Journal of Marine Research 54, 261–284.

Sarkisyan, A.S., Ivanov, V.F., 1971. Joint effect of baroclinicity and bottom relief as an important factor in the dynamics of sea currents. Izv. Academy of Science, USSR, Atmospheric and Oceanic Physics 7 (2), 173–188 (English translation).

Shaw, P.T., 1991. The seasonal variation of the intrusion of the Philippine Sea water into the South China Sea. Journal of Geophysical Research 96 (c1), 821–827.

Shaw, P.-T., Chao, S.-Y., 1994. Surface circulation in the South China Sea. Deep-Sea Research 41, 1663–1683.

Smagorinsky, J., 1963. General circulation experiments with primitive equations. I. The basic experiment. Monthly Weather Review 91, 99–164.

Wang, G., Chen, D., Su, J., 2006. Generation and life cycle of the dipole in the South China Sea summer circulation. Journal of Geophysical Research 111, C06002. doi:10.1029/2005JC003314.

Xu, X.Z.,Qiu, Z., Chen, H.C., 1982. The general descriptions of the horizontal circulation in the South China Sea. In: Proceedings of the 1980 Symposium on Hydrometeology of the Chinese Society of Oceanology and Limnology, Science Press, Beijing, pp. 137–145 (in Chinese with English abstract).

Xue, H., Chai, F., Pettigrew, N., Xu, D., Shi, M., Xu, J., 2004. Kuroshio intrusion and the circulation in the South China Sea. Journal of Geophysical Research 109, C02017. doi:10.1029/2002JC001724.

Yang, H.J., Liu, Q., Liu, Z., Wang, D., Liu, X., 2002. A general circulation model study of the dynamics of the upper ocean circulation of the South China Sea. Journal of Geophysical Research 107 (C7), 3085. doi:10.1029/2001JC001084.

Zhong, H.L., 1990. Density-related current structures. Report of 10-year Hydrographic Section Surveys of the Northern China Sea Continental Shelf Region and Adjacent Waters. China Ocean Press, Beijing, pp. 215–241 (in Chinese).